Soft Matter

Holographic Immunoassays: Direct Detection of Antibodies Binding to Colloidal Spheres

Journal:	*Soft Matter*
Manuscript ID	SM-ART-07-2020-001351.R1
Article Type:	Paper
Date Submitted by the Author:	15-Sep-2020
Complete List of Authors:	Snyder, Kaitlynn; New York University, Department of Physics Quddus, Rushna; New York University, Department of Chemistry Hollingsworth, Andrew; New York University, Department of Physics Kirshenbaum, Kent; New York University, Department of Chemistry Grier, David; New York University, Department of Physics

Soft Matter

ARTICLE TYPE

Cite this: DOI: 10.1039/xxxxxxxxxx

Holographic Immunoassays: Direct Detection of Antibodies Binding to Colloidal Spheres†

Kaitlynn Snyder,[a,‡] Rushna Quddus,[b,‡] Andrew D. Hollingsworth,[a] Kent Kirshenbaum,[b] and David G. Grier[a]

Received Date
Accepted Date

DOI: 10.1039/xxxxxxxxxx

www.rsc.org/journalname

The size of a probe bead reported by holographic particle characterization depends on the proportion of the surface area covered by bound target molecules and so can be used as an assay for molecular binding. We validate this technique by measuring the kinetics of irreversible binding for the antibodies immunoglobulin G (IgG) and immunoglobulin M (IgM) as they attach to micrometer-diameter colloidal beads coated with protein A. These measurements yield the antibodies' binding rates and can be inverted to obtain the concentration of antibodies in solution. Holographic molecular binding assays therefore can be used to perform fast quantitative immunoassays that are complementary to conventional serological tests.

1 Introduction: Holographic molecular binding assays

Holographic molecular binding assays use holographic particle characterization[1] to directly measure changes in the diameters of micrometer-scale colloidal spheres caused by molecules binding to their surfaces[2,3]. This rapid measurement technique eliminates the need for fluorescent labeling to detect binding and thus reduces the cost, complexity, time to completion and expertise required for standard binding assays such as ELISA. Being based on batch-synthesized beads, holographic molecular binding assays do not require microfabricated sensors and can be performed with comparatively little sample preparation. Holographic molecular binding assays therefore have great promise as medical diagnostic tests, particularly the serological tests required to assess patients' immune responses to pathogens such as SARS-CoV-2, the coronavirus responsible for COVID-19.

The ability to measure nanometer-scale changes in the diameters of micrometer-scale spheres is provided by quantitative analysis of single-particle holograms obtained with in-line holographic video microscopy[1,4]. The hologram of an individual colloidal sphere is fit to a generative model based on the Lorenz-Mie theory of light scattering[5–7] to extract the particle's diameter, d_p, refractive index, n_p and three-dimensional position, $\mathbf{r}_p$[1]. This measurement scheme is depicted schematically in Fig. 1. One such measurement can be completed in a few milliseconds and yields a bead's diameter with a precision of 5 nm and its refractive index to within 1 part per thousand[8]. A set of such measurements can be used to measure the mean diameter of a population of particles to within a fraction of a nanometer[3], which is sufficient to detect the growth of molecular-scale coatings.

Immunoassays based on holographic particle characterization are complementary to holographic viral-binding assays that recently were reported[9]. Those immunoassays use superresolution techniques to directly detect individual virions bound to functionalized substrates. Macromolecules, such as antibodies, cannot be detected in this way because they are too small.

Previous demonstrations of holographic molecular binding assays[2,3] have reported changes in probe beads' properties when the concentration of target molecules is large enough to saturate the beads' binding sites. Here, we report concentration-dependent trends that cover the range from zero analyte to binding-site saturation. Interpreting these results through the statistical mechanics of molecular binding then achieves three goals: (1) to use holographic binding assays to probe the kinetics of molecular binding; (2) to validate the effective-sphere model used to interpret holographic particle characterization measurements on coated spheres; and (3) to establish the effective range of analyte concentrations over which holographic binding assays can quantitate target molecules in solution, a key capability for clinical testing.

2 Experimental

We demonstrate quantitative holographic binding assays through measurements on antibodies binding to beads coated with protein A, specifically immunoglobulin G (IgG) and immunoglobulin

[a] Department of Physics and Center for Soft Matter Research, New York University, New York, NY 10003, USA
[b] Department of Chemistry, New York University, New York, NY 10003, USA
† Electronic Supplementary Information (ESI) available: The role of surface blocking in holographic immunoassays. See DOI: 10.1039/cXsm00000x/
‡ These authors contributed equally to this work.

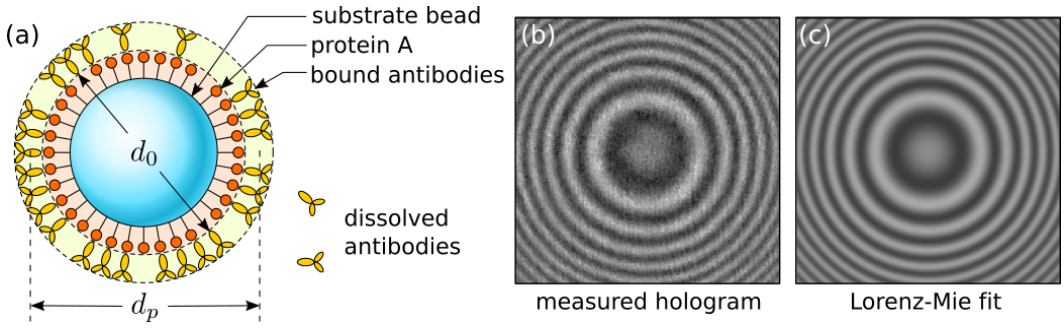

Fig. 1 (a) Schematic representation of a molecular binding assay based on holographic particle characterization. Probe beads consist of spherical polystyrene substrates coated with functional groups (protein A) that can bind target antibodies from solution. The probe beads have an effective diameter that increases from d_0 to d_p when antibodies bind. (b) A molecular-scale coating of antibodies influences the recorded hologram of a bead. (c) This change can be quantified by fitting to predictions of the Lorenz-Mie theory of light scattering, yielding an estimate for the fractional surface coverage and from this the concentration of antibodies.

M (IgM). These are well-studied model systems[10] with which to validate holographic binding assays and to establish their detection limits. Given the central role of IgG and IgM in the immune response to viral pathogens, these experimental demonstrations furthermore serve as models for fast, inexpensive and quantitative serological tests.

2.1 Probe beads and buffer solution

The probe beads used for this study (Bangs Laboratories, catalog no. CP02000, lot no. 14540) have a polystyrene core with a nominal diameter of $d_0 = 1\,\mu$m and a surface layer of immobilized protein A molecules, each of which has five binding sites for the Fc region of immunoglobulins[11,12]. These functionalized beads are dispersed at a concentration of 2×10^6 particles/mL in an antibody binding buffer. The same buffer is used to dissolve antibodies for testing. Equal volumes of the probe-bead dispersion and the antibody solution are mixed to initiate incubation.

The antibody binding buffer consists of 50 mM sodium borate buffer prepared with boric acid (99.5 %, Sigma-Aldrich, catalog no. B0394, lot no. SLBM4465V) and NaOH (98 %, Sigma-Aldrich, catalog no. S8045, lot no. 091M01421V) in deionized water (18.2 MΩcm, Barnstead Millipure). The pH of the buffer is adjusted to 8.2 with the addition of dilute HCl (38 %, Sigma-Aldrich, catalog no. H1758) to optimize the binding of antibodies to protein A[13].

The dispersion of functionalized colloidal spheres constitutes a bead-based assay kit for immunoglobulins that bind to protein A. The same approach can be used to create specific immunoassays for particular antibodies by functionalizing the beads' surfaces with suitable antigens instead of protein A. Multiplexed assays can be produced by separately functionalizing substrate beads that can be distinguished holographically by size or by refractive index and then mixing their dispersions to make a test kit.

2.2 Assay protocol

An assay is performed by dissolving target antibodies in the buffer at concentrations from 200 ng mL^{-1} up to 200 μg mL^{-1}. Antibody solution is then mixed with an equal volume of the stock dispersion of probe beads to obtain a bead concentration of 10^6 particles/mL and antibody concentrations in the range from 100 ng mL^{-1} to 100 μg mL^{-1}. This easily allows for detection in a physiologically relevant range following suitable dilution, as the typical concentration of immunoglobulins in human serum is 10 mg mL^{-1} [14]. The sample is allowed to equilibrate for $\tau = 45$ min at room temperature before being analyzed.

To model immunoassays that would be relevant for serological testing, we performed assays on rabbit IgG (EMD Millipore; catalog no. PP64, lot no. 3053798) and human IgM (Sigma-Aldrich; catalog no. I8260, lot no. 069M4838V). Aggregation of IgM is suppressed by increasing the ionic strength of the buffer through the addition of 150 mM of NaCl (99.5 %, Sigma-Aldrich, catalog no. S7653)[15].

Control measurements are performed by replacing the antibodies with alcohol dehydrogenase (ADH, Sigma-Aldrich; catalog no. A3263-7.5KU, lot no. SLBW31382). Non-specific binding due to incomplete coverage of the bead surfaces by protein A is blocked[†] for these experiments by incubating the probe beads with bovine serum albumin (BSA, Sigma-Aldrich, catalog no. A2153). BSA adsorbs non-specifically to exposed polystyrene and does not interfere with antibody binding to protein A. ADH does not bind to either protein A or BSA and thus should not attach to the probe beads. With a molecular weight greater than 140 kDa, ADH is comparable in size to IgG and thus should have a similar holographic signature, were it to bind.

2.3 Holographic particle characterization

Holographic particle characterization measurements are performed with a commercial holographic particle characterization instrument (Spheryx xSight) set to record holograms at a wavelength of 447 nm. Each measurement involves pipetting a 30 μL aliquot of the dispersion into the sample reservoir of one channel in an eight-channel microfluidic chip (Spheryx xCell). The sample chip is then loaded into xSight, which is set to draw 1 μL of the sample through the observation volume in a pressure-driven flow with a peak speed of 3 mm s^{-1}. Data for a thousand beads is collected in measurement time $\Delta\tau = 2$ min and is fully analyzed in about 15 min.

The Lorenz-Mie theory used to analyze holograms treats each

particle as a homogeneous sphere. When applied to inhomogeneous particles, such as the coated spheres in the present study, the extracted parameters must be interpreted as representing the properties of an effective sphere[16–18]. These effective-sphere properties will differ from the physical properties of the coated sphere unless the coating has the same refractive index as the substrate bead. The refractive index of the coating, moreover, depends on the fraction, f, of binding sites occupied by molecules, which means that the effective diameter of the coated sphere also depends on f. Numerical studies show that the holographically measured diameter increases linearly with surface coverage[18],

$$d_p = d_0 + 2\delta f, \tag{1}$$

where d_0 is the probe sphere's diameter and δ is the effective optical thickness of a complete layer of bound molecules. The value of δ depends on the size of the target molecule, the density of binding sites, and the refractive index of the target molecule relative to those of the medium and the substrate bead[18].

Each dispersed particle is recorded and analyzed up to 10 times as it traverses the observation volume and the resulting three-dimensional position measurements are linked into a trajectory[19]. Dividing the length of a single-particle trajectory by the duration of the particle's transit through the observation volume yields the particle's speed, $v_p(z_p)$, as a function of its axial position, z_p, relative to the instrument's focal plane. The same observations also yield multiple independent measurements of the particle's diameter and refractive index that are combined to improve the precision of the estimated values[2].

Typical results for a sample of beads incubated with $10\,\mu\mathrm{g\,mL^{-1}}$ of IgG are presented in Fig. 2. Each point in these scatter plots represents one particle's trajectory, Fig. 2(a), and physical properties, Fig. 2(b). The size of the dots is comparable to the estimated single-particle measurement precision[1].

The distribution of trajectory data in in Fig. 2(a) maps the flow field in the microfluidic channel[2]. The individual points are colored by the spheres' measured diameters. The random distribution of colors confirms that particles are distributed uniformly throughout the channel and that particle size is not correlated with height in the channel. Fitting these data to the anticipated parabolic Poiseuille flow profile yields estimates for the positions of the upper and lower walls of the channel, which are indicated by the horizontal dashed lines in Fig. 2(a). This part of the analysis provides a useful quality control check by ensuring that the sample has flowed smoothly through the channel, that the microfluidic channel is properly seated in the instrument, and that trajectory linking has proceeded correctly.

Figure 2(b) shows the single-particle characterization data obtained from these trajectories, with each point representing the effective diameter, d_p, and refractive index, n_p, of a single bead. Plot symbols are colored by the density of observations, $\rho(d_p, n_p)$. The 890 particles in this data set enable us to compute the population-average diameter, $d_p = (0.974 \pm 0.002)\,\mu$m and the mean refractive index, $n_p = 1.570 \pm 0.001$. We can compare these with the corresponding values for the probe beads before incubation, $d_0 = (0.964 \pm 0.002)\,\mu$m and $n_0 = 1.571 \pm 0.002$. Although incubation with IgG appears not to have changed the beads' refractive index significantly, their mean diameter has increased by $\Delta_d = d_p - d_0 = (10 \pm 3)\,$nm.

The values obtained for the physical properties of the beads are reasonable. The baseline value for the probe beads' mean diameter is consistent with the manufacturer's specification, $0.95\,\mu\mathrm{m} \leq d_0 \leq 1.05\,\mu$m. The value for the refractive index is significantly smaller than the value of 1.60 expected for polystyrene at the imaging wavelength, and is consistent with expectations for a coated sphere in the effective-sphere interpretation[18].

The uncertainties in the mean diameters, d_p and d_0, depend on the widths of the underlying diameter distributions, which we estimate with the standard deviation of the set of observed diameters. The precision with which the centers of those distributions can be estimated depends on the size of the statistical sample. The reported uncertainties are the computed standard deviations divided by the square root of the number of observations. Smaller uncertainties therefore can be obtained by starting with more monodisperse probe particles and by measuring more of them.

The observed increase in bead diameter is consistent with a statistically significant detection of antibody binding[3] at concentrations two to three orders of magnitude lower than physiological levels[14,20–22]. A principal aim of the present study is to combine the effective-sphere analysis of probe beads' holograms[2,3,18] with the statistical physics of molecular binding to obtain quantitative information on the kinetics of antibody binding from measurements of $d_p(c,t)$. Conversely, this analysis establishes that a holographically observed shift in bead diameter can be used to measure the concentration of antibodies in solution and furthermore establishes the trade-off between concentration sensitivity and measurement time for such holographic immunoassays.

2.4 Kinetics of molecular binding

Antibodies bind rapidly to protein A in the antibody binding buffer and the rate of dissociation is small enough for the process to be considered irreversible[23]. Antibodies therefore continue to bind to the probe beads until all of the surface sites are saturated or the solution is depleted. Assuming that depletion may be ignored and the solution remains well mixed, the fraction of occupied sites, $f(c,t)$, increases at a rate that depends on the concentration of antibodies, c, and the availability of unoccupied sites[24–26]

$$\frac{df}{dt} = \gamma(c)[1 - f(c,t)]. \tag{2}$$

This model differs from those in previous studies[27–29] by not having to account for detachment of antibodies from binding sites. Minimizing unbinding optimizes the sensitivity of the assay to small concentrations of analyte and reduces the time required to perform measurements.

The rate constant, $\gamma(c)$, accounts for the microscopic kinetics of molecular binding. Further assuming that the concentration of antibodies is low enough that binding events are independent, we model $\gamma(c) = kc$, where k is the binding rate for the antibodies in

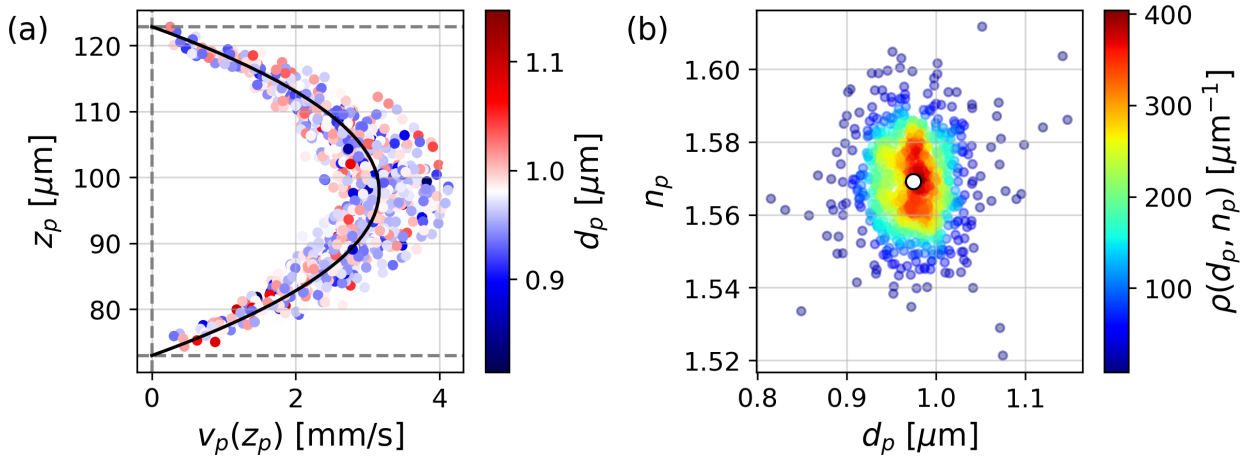

Fig. 2 Typical holographic molecular binding assay for a sample of probe beads incubated with $10\,\mu\mathrm{g\,mL^{-1}}$ IgG. (a) Holographically measured velocity profile. Each point represents the speed, v_p, of a single bead as a function of its axial position, z_p, relative to the instrument's focal plane. The solid curve is a fit to the parabolic Poiseuille flow profile. Horizontal dashed lines indicate the axial positions of the channel's walls inferred from this fit. Points are colored by each particle's measured diameter, d_p. Evenly mixed colors demonstrate that the results are not biased by the particles' positions in the channel. (b) Holographic characterization data for the same sample of beads showing the distribution of single-particle diameter, d_p, and refractive index, n_p. Points are colored by the density of measurements, $\rho(d_p,n_p)$. The central point shows the population mean for this sample and is sized to represent the uncertainty in the mean.

the antibody binding buffer. The solution to Eq. (2),

$$f(c,t) = 1 - e^{-kct}, \tag{3}$$

satisfies the initial condition $f(c,0) = 0$ and shows that binding assays can be performed either as a function of time for fixed antibody concentration, c, or as a function of concentration at fixed incubation time, t. If, furthermore, the measurement is performed over a time interval, $\Delta\tau$, starting after incubation time τ, the average coverage is

$$\bar{f}(c,\tau) = \frac{1}{\Delta\tau}\int_{\tau}^{\tau+\Delta\tau} f(c,t)\,dt \tag{4a}$$

$$= 1 - \frac{1-e^{-kc\Delta\tau}}{kc\Delta\tau}\,e^{-kc\tau}. \tag{4b}$$

2.5 Monitoring binding holographically

Combining Eq. (1) with Eq. (4) yields an expression for the dependence of the measured bead diameter on the target molecules' concentration in solution:

$$\Delta_d(c,\tau) \equiv d_p - d_0 = 2\delta\left(1 - \frac{1-e^{-kc\Delta\tau}}{kc\Delta\tau}\,e^{-kc\tau}\right). \tag{5}$$

Holographic measurements of $\Delta_d(c,\tau)$ at fixed incubation time τ can be interpreted with Eq. (5) to estimate the effective layer thickness, δ, and the rate constant, k. These values, in turn, can be used to anticipate how the sensitivity of the assay for antibody concentration depends on incubation time, τ. This sensitivity can be further improved by reducing uncertainties in $\Delta_d(c,\tau)$, either by extending the measurement time to analyze more beads or by optimizing the optical properties of the beads to increase δ[18].

3 Results & Discussion

The discrete points in Fig. 3 show measured shifts, $\Delta_d(c,\tau)$, in the population-average bead diameter after $\tau = 45\,\mathrm{min}$ incubation with (a) IgG, (b) IgM and (c) ADH. These shifts are measured in nanometers and illustrate the precision with which holographic particle characterization can resolve the diameters of probe beads. Error bars reflect uncertainties, σ_Δ, in Δ_d, obtained as the quadrature sum of the uncertainties in d_0 and d_p. Each single point represents results from roughly 1000 beads observed in $1\,\mu\mathrm{L}$ of the sample over $\Delta\tau = 2\,\mathrm{min}$.

As anticipated, bead diameters increase upon incubation with antibodies by an amount that depends on antibody concentration. Incubation with ADH has no such effect, presumably because ADH does not bind to protein A. Results for IgG and ADH are presented for concentrations up to $100\,\mu\mathrm{g\,mL^{-1}}$. IgM is plotted only up to $20\,\mu\mathrm{g\,mL^{-1}}$ because $\Delta_d(c,t)$ reaches a plateau beyond $c = 5\,\mu\mathrm{g\,mL^{-1}}$, which we interpret to represent saturation of the available surface sites by IgM.

The threshold sensitivity is the concentration, c_{min}, beyond which the measured diameter increase exceeds the uncertainty,

$$\Delta_d(c_{\mathrm{min}}) \geq \sigma_\Delta. \tag{6}$$

For IgG, this yields $c_{\mathrm{min}} = 10\,\mu\mathrm{g\,mL^{-1}}$. The corresponding threshold for IgM is $c_{\mathrm{min}} = 1\,\mu\mathrm{g\,mL^{-1}}$.

The solid curves in Fig. 3(a) and Fig. 3(b) are fits of the measured bead diameters to Eq. (5) for the apparent layer thickness, δ, and the rate constant, k. Interestingly, fits to the data for both IgG and IgM are consistent with an effective layer thickness of $\delta = (8.0 \pm 0.5)\,\mathrm{nm}$ even though IgM has five times the molecular weight of IgG. This agreement could be a coincidence arising from the effective-sphere interpretation of holographic imaging data[18]. It also is consistent with a model in which multi-site

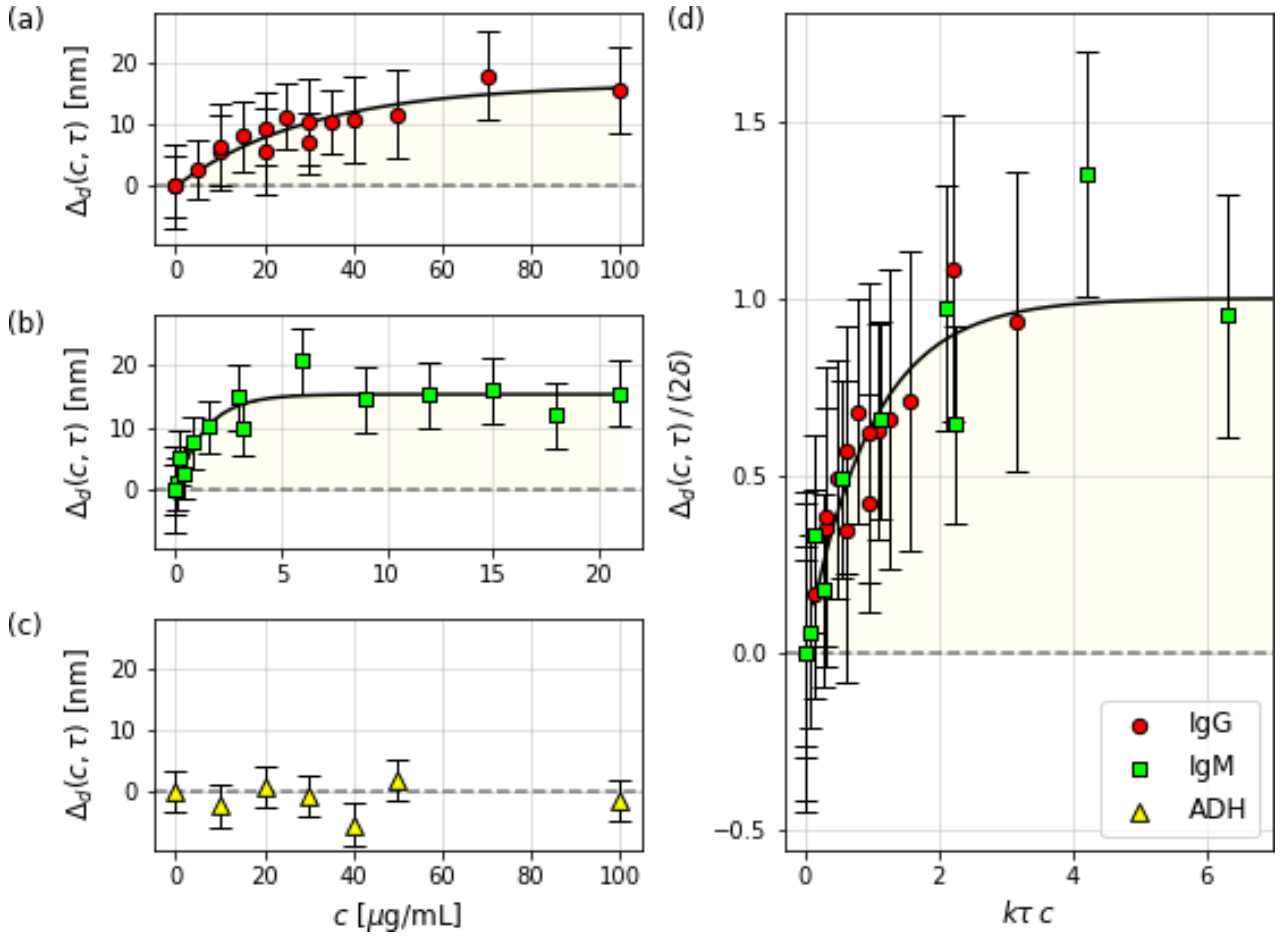

Fig. 3 Holographic molecular binding assays for (a) IgG (red circles) and (b) IgM (green squares) to colloidal beads coated with protein A dispersed in antibody binding buffer. IgM assay is performed with 150 mM added NaCl to suppress aggregation. Discrete points show the increase, $\Delta_d(c,\tau) = d_p(c,\tau) - d_0$, of the population-average effective-sphere diameter, $d_p(c,\tau)$, relative to the probe beads' reference diameter, d_0, as a function of antibody concentration, c after fixed incubation time $\tau = 45$ min. Each data point represents an average of 1000 beads and is replicated three times. Solid curves are best-fits to Eq. (5) for measurement time $\Delta\tau = 2$ min. (c) 45 minute incubation with alcohol dehydrogenase (ADH) has no measurable affect on probe bead diameters. (d) Binding data collapsed according to Eq. (5). Concentrations are scaled by $k\tau$ and diameter shifts are scaled by the layer thickness, δ.

binding of the predominantly pentameric IgM assembly results in a flattened orientation of the IgM on the probe beads' surfaces, thus contributing no more to δ than the single domain of IgG. This interpretation is supported by independent cryo-AFM studies that show IgM pentamers consistently lying flat upon mica surfaces, thereby forming monolayers less than 10 nm thick[30].

The fit value for the rate constant of IgG is $k_G = (1.8 \pm 0.5) \times 10^3\,\mathrm{M^{-1}\,s^{-1}}$, given the 150 kDa molecular weight of IgG. This should be interpreted as a rate per binding site on the surface of a sphere. The value is consistent with results obtained independently with a surface acoustic waveguide device using protein A immobilized on a gold surface[31].

The corresponding rate constant for IgM, $k_M = (2.5 \pm 0.8) \times 10^5\,\mathrm{M^{-1}\,s^{-1}}$, is two orders of magnitude larger, taking the mass of pentameric IgM to be 970 kDa. Naively assuming that each IgG molecules occupies $\nu_G = 1$ binding site and each IgM occupies $\nu_M = 5$ reduces the difference proportionately,

$$\frac{k_M}{\nu_M}\frac{\nu_G}{k_G} = 28 \pm 12. \qquad (7)$$

The remaining large difference in binding rates cannot be ascribed to differences in bulk transport properties because the molecules' diffusion constants are proportional to their sizes, which suggests that IgG should attach more rapidly, being smaller. It may instead reflect differences in the two antibodies' microscopic binding mechanisms[32]. Possible explanations include differences in binding probabilities as molecules approach the surface due to the multivalent presentation of binding sites for the pentameric IgM. In addition, different barriers to attachment may arise due to variations in the nature of electrostatic interactions for immunoglobulins. A more thorough evaluation of the influence of multivalency on attachment kinetics for IgGs, IgMs and other biomacromolecules will provide an intriguing application area for holographic immunoassays. Even a simplified model such as the one-to-one binding model between protein A and IgG considered here provides a practical basis for measuring immunoglobulin concentration in solution.

Given our primary goal of developing rapid and inexpensive immunoassays for serological testing, the experimental results in

Fig. 3 confirm that holographic particle characterization provides a basis for quantitative measurements of antibody concentrations under physiological conditions. The success of these fits to a kinetic model for attachment is demonstrated by the data collapse in Fig. 3(d), with results from IgG and IgM both falling on the same master curve despite the 140-fold difference in the two antibodies' binding rate constants.

4 Conclusions

This study has demonstrated that holographic particle characterization can perform quantitative molecular binding assays, including measuring the rate constants that characterize molecular binding. Our results demonstrate that a single 15 min measurement can quantify the concentration of IgG in solution down to concentrations as low as $10\,\mu g\,mL^{-1}$ and concentrations of IgM as low as $1\,\mu g\,mL^{-1}$. These limits are three orders of magnitude smaller than the standard physiological concentrations of $7\,mg\,mL^{-1}$ to $16\,mg\,mL^{-1}$ for IgG and $0.4\,mg\,mL^{-1}$ to $2.3\,mg\,mL^{-1}$ for IgM[20] in healthy people. Still smaller concentrations can be monitored with longer measurements and larger statistical samples.

Whereas the IgG-protein A system has been studied extensively, less is known regarding binding of IgM to substrates coated with protein A. The holographic assays reported here provide insights into the binding mechanism that may inform future studies. We find, for example, that IgM tends to bind significantly more rapidly to protein A than IgG. Our observations also suggest that IgM may tend to bind flat to the surface of a functionalized bead. How these trends depend on such factors as electrolyte composition and concentration fall outside the intended scope of the present study and will be addressed elsewhere.

Using protein A to provide binding functionalization yields a general-purpose assay for antibody concentration, rather than an immunoassay for specific antibodies. This general-purpose assay already should be useful as a rapid screening test for Antibody Deficiency Disorders[33,34].

Holographic immunassays can be targeted for specific diseases by replacing protein A as a surface binding group with appropriate specific antigens, including peptides, proteins, or other biomolecules. Such functionalized colloidal spheres are standard components of conventional bead-based assays, which typically rely on fluorescent labels for readout. Holographic analysis yields results faster and at lower cost by eliminating reagents, processing steps and expertise needed to apply fluorescent labels. Holographic analysis furthermore yields quantitative results for antibody concentration without requiring extensive calibration. The speed and sensitivity of holographic immunoassays can be improved further by optimizing the sizes and optical properties of the substrate beads. Such efforts currently are under way.

5 Conflicts of Interest

D.G.G. is a founder of Spheryx, Inc., which manufacturers the xSight instrument used in this work.

6 Acknowledgements

This work was supported by the RAPID program of the National Science Foundation under Award No. DMR-2027013. Partial support was provided by NASA through Grant No. NNX13AR67G. The Spheryx xSight holographic characterization instrument used in this study was acquired by New York University's Materials Research Science and Engineering Center as shared instrumentation with support from the NSF under Award No. DMR-1420073.

Notes and references

1 S.-H. Lee, Y. Roichman, G.-R. Yi, S.-H. Kim, S.-M. Yang, A. Van Blaaderen, P. Van Oostrum and D. G. Grier, *Opt. Express*, 2007, **15**, 18275–18282.
2 F. C. Cheong, B. S. R. Dreyfus, J. Amato-Grill, K. Xiao, L. Dixon and D. G. Grier, *Opt. Express*, 2009, **17**, 13071–13079.
3 Y. Zagzag, M. F. Soddu, A. D. Hollingsworth and D. G. Grier, *Sci. Rep.*, 2020, **10**, 1–7.
4 J. Sheng, E. Malkiel and J. Katz, *Appl. Opt.*, 2006, **45**, 3893–3901.
5 M. I. Mishchenko, L. D. Travis and A. A. Lacis, *Scattering, Absorption, and Emission of Light by Small Particles*, Cambridge University Press, 2002.
6 C. F. Bohren and D. R. Huffman, *Absorption and Scattering of Light by Small Particles*, John Wiley & Sons, 2008.
7 G. Gouesbet and G. Gréhan, *Generalized Lorenz-Mie theories*, Springer, 2011, vol. 31.
8 B. J. Krishnatreya, A. Colen-Landy, P. Hasebe, B. A. Bell, J. R. Jones, A. Sunda-Meya and D. G. Grier, *Am. J. Phys.*, 2014, **82**, 23–31.
9 A. Ray, M. U. Daloglu, J. Ho, A. Torres, E. Mcleod and A. Ozcan, *Sci. Rep.*, 2017, **7**, 1–9.
10 L. N. Lund, T. Christensen, E. Toone, G. Houen, A. Staby and P. M. St. Hilaire, *J. Mol. Recognit*, 2011, **24**, 945–952.
11 J. Deisenhofer, *Biochem.*, 1981, **20**, 2361–2370.
12 T. Moks, L. Abramsén, B. Nilsson, U. Hellman, J. Sjöquist and M. Uhlén, *Eur. J. Biochem.*, 1986, **156**, 637–643.
13 J. B. Fishman and E. A. Berg, *Cold Spring Harbor Protocols*, 2019, **2019**, pdb–prot099143.
14 J. T. Cassidy and G. L. Nordby, *J. Allergy Clin. Immunol.*, 1975, **55**, 35–48.
15 J. B. Fishman and E. A. Berg, *Cold Spring Harbor Protocols*, 2019, **2019**, pdb–top099101.
16 F. C. Cheong, K. Xiao, D. J. Pine and D. G. Grier, *Soft Matter*, 2011, **7**, 6816–6819.
17 M. A. Odete, F. C. Cheong, A. Winters, J. J. Elliott, L. A. Philips and D. G. Grier, *Soft Matter*, 2020, **16**, 891–898.
18 L. E. Altman and D. G. Grier, *Biomed. Opt. Express*, 2020, **11**, 5225–5236.
19 J. C. Crocker and D. G. Grier, *J. Colloid Interface Sci.*, 1996, **179**, 298–310.
20 F. Dati, G. Schumann, L. Thomas, F. Aguzzi, S. Baudner, J. Bienvenu, O. Blaabjerg, S. Blirup-Jensen, A. Carlström and P. Hyltoft-Petersen, *Euro. J. Clin. Chem. Clin. Biochem.*, 1996, **34**, 517–520.

21 M. F. Goldstein, A. L. Goldstein, E. H. Dunsky, D. J. Dvorin, G. A. Belecanech and K. Shamir, *Ann. Allerg. Asthma Im.*, 2006, **97**, 717–730.

22 Q.-X. Long, B.-Z. Liu, H.-J. Deng, G.-C. Wu, K. Deng, Y.-K. Chen, P. Liao, J.-F. Qiu, Y. Lin, X.-F. Cai *et al.*, *Nature Med.*, 2020, 1–4.

23 W. Norde, *J. Disper. Sci. Technol.*, 1992, **13**, 363–377.

24 V. Privman, J.-S. Wang and P. Nielaba, *Phys. Rev. B*, 1991, **43**, 3366.

25 J. Buijs, P. A. van den Berg, W. T. James, W. Norde, J. Lyklema *et al.*, *J. Colloid Interface Sci.*, 1996, **178**, 594–605.

26 Z. Adamczyk, *J. Colloid Interface Sci.*, 2000, **229**, 477–489.

27 K.-P. S. Dancil, D. P. Greiner and M. J. Sailor, *J, Am. Chem. Soc.*, 1999, **121**, 7925–7930.

28 H. Ogi, K. Motohisa, K. Hatanaka, T. Ohmori, M. Hirao and M. Nishiyama, *Biosens. Bioelectron.*, 2007, **22**, 3238–3242.

29 J. T. Nelson, S. Kim, N. F. Reuel, D. P. Salem, G. Bisker, M. P. Landry, S. Kruss, P. W. Barone, S. Kwak and M. S. Strano, *Anal. Chem.*, 2015, **87**, 8186–8193.

30 D. M. Czajkowsky and Z. Shao, *Proc. Nat. Acad. Sci.*, 2009, **106**, 14960–14965.

31 K. Saha, F. Bender and E. Gizeli, *Anal. Chem.*, 2003, **75**, 835–842.

32 E. C. Y. Law, D. T. M. Leung, F. C. H. Tam, K. K. T. Cheung, N. H. Y. Cheng and P. L. Lim, *Front. Immunol.*, 2019, **10**, 1820.

33 M. Ballow, *J. Allergy Clin. Immunol.*, 2002, **109**, 581–591.

34 S. Y. Patel, J. Carbone and S. Jolles, *Front. Immunol.*, 2019, **10**, 33.

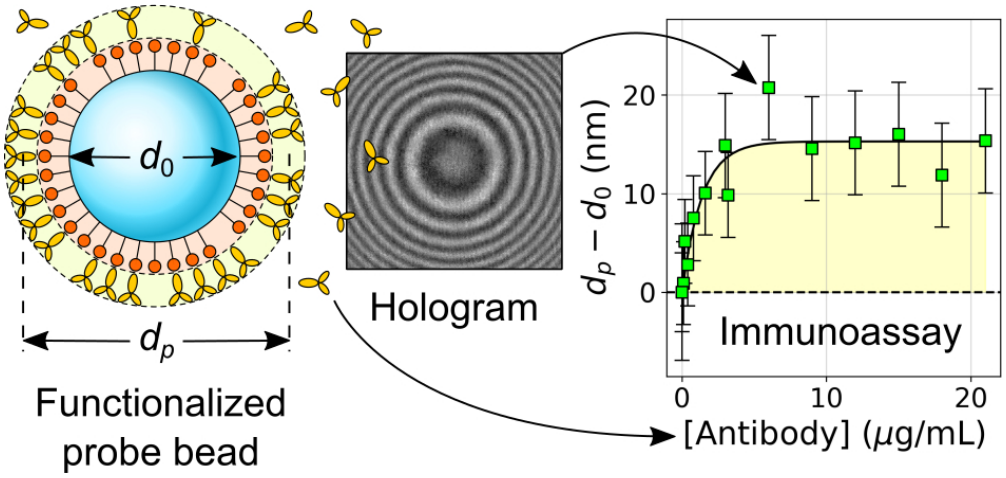
d_0
d_p
Functionalized
probe bead
Hologram
$d_p - d_0$ (nm)
20
10
0
0
10
20
Immunoassay
[Antibody] (μg/mL)